PHYSICAL REVIEW B **83**, 220508(R) (2011)

Relation between nodes and $2\Delta/T_c$ on the hole Fermi surface in iron-based superconductors

Saurabh Maiti and Andrey V. Chubukov
Department of Physics, University of Wisconsin, Madison, Wisconsin 53706, USA
(Received 14 April 2011; revised manuscript received 16 May 2011; published 16 June 2011)

We analyze the interplay between the absence or presence of nodes in the superconducting gap along electron Fermi surfaces (FSs) in Fe pnictides and $2\Delta/T_c$ along hole FSs ($2\Delta_h/T_c$), measured by angle-resolved photoemission spectroscopy (ARPES). We solve the set of coupled gap equations for 4- and 5-pocket models of Fe pnictides and relate the presence of the nodes to $2\Delta_h/T_c$ being below a certain threshold. Using ARPES data for $2\Delta_h/T_c$, we find that the optimally doped $Ba_{1-x}K_xFe_2As_2$ and $Ba(Fe_{1-x}Co_x)_2As_2$ are likely nodeless, but isovalent $BaFe_2(As_{1-x}P_x)_2$ likely has nodes.

DOI: 10.1103/PhysRevB.83.220508 PACS number(s): 74.20.Rp, 74.70.Xa

Introduction. The properties of Fe-based superconductors (FeSC) continue to attract interest in the condensed matter community. Amongst them, the pairing symmetry and the gap structure are the most debated topics. FeSCs are multiorbital/multiband quasi-2D systems, with two cylindrical hole pockets centered at (0,0), and two cylindrical electron pockets at $(\pi,0)$ and $(0,\pi)$ in the unfolded Brillouin zone (BZ) with one Fe atom per unit cell. In some systems, there is an additional cylindrical hole pocket at (π,π). This Fermi-surface (FS) topology allows several different gap symmetries and structures: s^{++} and $s^{\pm}$ s-wave states, $d_{x^2-y^2}$ and d_{xy} states, etc.[1–5] Most of theoretical and experimental studies[4,6–12] favor an $s\pm$ state in which the gaps averaged along the electron and hole pockets are of opposite sign. The $s\pm$ gap generally has some $\pm\cos 2\theta$ variations along the two electron FSs and has accidental nodes when such a variation is large. Penetration depth and thermal conductivity data indicate that in some of the FeSCs the gap probably has no nodes,[13–15] while in others accidental nodes are likely. The most compelling evidence for the nodes is for the strongly doped $Ba(Fe_{1-x}Co_x)_2As_2$,[13,16] $LaFeAsO_{1-x}F_x$,[17] and for the isovalent $BaFe_2(As_{1-x}P_x)_2$.[18]

The nodes in the gap can be directly probed by angle-resolved photoemission (ARPES). ARPES measures the gaps in the folded BZ, where the three hole FSs are all at (0,0) and the two electron FSs are both at (π,π). At present, ARPES measurements distinguish between the gaps on the hole FSs, but cannot resolve the two gaps on the electron FSs (a possible exception is the hole-doped $Ba_{1-x}K_xFe_2As_2$[19]). The issue of the resolution is relevant because $\cos 2\theta$ modulations of the gaps on the two electron FSs have π phase shift, and the convoluted (unresolved) gap remains a constant along the electron FS even if each of the two gaps has nodes.

Both conventional and laser ARPES measurements[19–26] have shown that the gaps on the hole FSs, Δ_h, are weakly angle dependent, but $2\Delta_h/T_c$ differs from the BCS value of 3.53 (see Ref. 27). The issue we discuss in this communication is whether one can make a prediction, based on these measured $2\Delta_h/T_c$, about the presence or absence of the gap nodes on the electron FSs. We consider 4- and 5-pocket models of FeSCs and argue that, if the largest $2\Delta_h/T_c$ is below or above a threshold value (different for 4- and 5-pocket models), the electron gaps either definitely have nodes or definitely have no nodes, respectively. There is a "gray" area for $2\Delta_h/T_c$ around the threshold, when the electron gap is either nodal or non-nodal, depending on the parameters, but this gray area is rather narrow.

Method. We ignore 3D effects, the potential hybridization of electron FSs in the folded BZ, and the difference between the densities of states, N_F, in different FSs, and focus on the two key features associated with the multiorbital and multiband nature of FeSCs: the presence of multiple FS pockets and the angle dependencies of the interactions between low-energy fermions due to variation of the orbital character along the FSs. In the band basis, this variation is passed onto the interactions that become angle dependent. We project the interactions onto an s-wave channel, solve the coupled set of nonlinear gap equations for the gaps along hole and electron FSs. and relate $2\Delta_h/T_c$ to the strength of the $\cos 2\theta$ component of the electron gap.

We make several simplifying assumptions aiming to reduce the number of input parameters. First, we keep the angular dependence of electron-hole interaction, $u_{eh}(\theta)$, and approximate the hole-hole and electron-electron interactions with constants. This is in line with the earlier study,[28] which found that the structure of $s^{\pm}$ gap is chiefly determined by the angle dependence of $u_{eh}(\theta)$. Second, we keep only the leading 2θ harmonic in u_{eh}: $u_{eh} = u_{eh}(1 \pm 2\alpha\cos 2\theta)$, where different signs are for different electron FSs (for justification see Refs. 28–30). Third, we take the ratios of different intraband and interband hole-hole, electron-electron, and hole-electron interactions to be the values to which they flow under renormalization group (RG) flow.[29] This leaves us with just three parameters: u_{eh}, α, and the magnitude of intrapocket hole-hole interaction, u_{hh}. Other hole-hole and electron-electron interactions scale as u_{hh} with the prefactors (different in different models) set by the RG flow.[29] The overall magnitude of the interaction doesn't affect $2\Delta_h/T_c$ in the BCS limit that we consider, hence, the actual number of input parameters is two: α and $\beta \equiv u_{hh}/u_{eh}$. We solve the nonlinear gap equations for 4- and 5-pocket models in two limits: (i) when the two hole FSs centered at (0,0) in the unfolded BZ are equal (model A) and (ii) when only one hole FS at (0,0) is present (model B). These choices are dictated by our desire to minimize the number of input parameters and at the same time to understand a generic case of two nonequivalent hole FSs at (0,0), which should be a case in between the two limits.

The gap structure for $u_{eh} = u_{eh}(1 \pm 2\alpha \cos 2\theta)$ is given by

$$\Delta_h^{(0,0)}(\mathbf{k}) = \Delta_{h_1}, \Delta_h^{(\pi,\pi)}(\mathbf{k}) = \Delta_{h_2},$$
$$\Delta_e^{(\pi,0)}(\mathbf{k}) \text{ and } \Delta_e^{(0,\pi)}(\mathbf{k}) = \Delta_{e_1} \pm \Delta_{e_2} \cos 2\theta. \quad (1)$$

For briefness, we discuss our computational procedure for the model A for the 4-pocket case. The computations for other models are similar.

The set of coupled BCS-type equations at T=0 is obtained by conventional means and reads:

$$\Delta_h = -4\beta u_{he} \Delta_h \log \frac{2\Lambda}{|\Delta_h|} - 2u_{he} \int \frac{d\theta}{2\pi}(1 + 2\alpha \cos 2\theta)\Delta_e(\theta) \log \frac{2\Lambda}{|\Delta_e(\theta)|}, \quad (2)$$

$$\Delta_{e_1} = -4u_{he}\Delta_h \log \frac{2\Lambda}{|\Delta_h|} - 4\beta u_{he} \int \frac{d\theta}{2\pi} \Delta_e(\theta) \log \frac{2\Lambda}{|\Delta_e(\theta)|},$$
$$\Delta_{e_2} = -8\alpha u_{he}\Delta_h \log \frac{2\Lambda}{|\Delta_h|},$$

where $\Delta_e(\theta) = \Delta_{e_1} + \Delta_{e_2} \cos 2\theta$ and Λ is the upper cutoff. We treat u_{he} as dimensionless, meaning that it is the product of the actual interaction and N_F.

The conventional route to find $2\Delta/T_c$ is to solve first the linear gap equation, express u_{he} in terms of T_c, substitute the result into the nonlinear gap equation, and obtain the closed-form equation for $\tilde{\Delta}_i \equiv \gamma \Delta_i / \pi T_c$ ($\log \gamma \approx 0.577$). For one-band BCS superconductor this yields $\log \tilde{\Delta} = 0$, i.e., $2\Delta/T_c = 2\pi/\gamma = 3.53$. For a multiband superconductor, $2\Delta/T_c$ differs from the value of 3.53 for two reasons: (1) because the hole and electron gaps are different and (2) because the ratios between the gaps change by $O(u_{eh})$ between T_c and $T = 0$. To account for both effects, we introduce $\Delta_{e_1} = \gamma_1 \Delta_h$ and $\Delta_{e_2} = \gamma_2 \Delta_h$ and write $\gamma_1 = \gamma_1^o + u_{he}\gamma_1^{(1)}$ and $\gamma_2 = \gamma_2^o + u_{he}\gamma_2^{(1)}$, where $\gamma_{1,2}^o$ are the values of $\gamma_{1,2}$ at T_c. The set of linearized gap equations at T_c reduces to equations on $u_{he} \log \gamma \Lambda/\pi T_c$ and $\gamma_{1,2}^o$:

$$\left[\mathbf{1} + \begin{pmatrix} 4\beta & 2 & 2\alpha \\ 4 & 4\beta & 0 \\ 8\alpha & 0 & 0 \end{pmatrix} u_{he} L \right] \begin{bmatrix} 1 \\ \gamma_1^o \\ \gamma_2^o \end{bmatrix} = 0, \quad (3)$$

where $L = \ln(\gamma \Lambda/\pi T_c)$. Solving Eq. (3), we obtain γ_1^o and γ_2^o as functions of α and β. We then substitute the solutions into Eq. (2), collect the terms $O(u_{he})$, and obtain a set of three equations on $\tilde{\Delta}_h$, $\gamma_1^{(1)}$, and $\gamma_2^{(1)}$, with α and β as parameters:

$$\begin{pmatrix} 1 & 2l & 2\alpha l \\ \gamma_1^o & 1 + 4\beta l & 0 \\ \gamma_2^o & 0 & 1 \end{pmatrix} \begin{pmatrix} a \log \tilde{\Delta}_h \\ \gamma_1^{(1)} \\ \gamma_2^{(1)} \end{pmatrix} = - \begin{pmatrix} 2\chi_1 \\ 4\beta\chi_2 \\ 0 \end{pmatrix}, \quad (4)$$

where $a = -(8\alpha)/\gamma_2^0$, and

$$\chi_1 = \int \frac{d\theta}{2\pi}(1 + 2\alpha \cos 2\theta)\left(\gamma_1^o + \gamma_2^o \cos 2\theta\right) L_\gamma,$$
$$\chi_2 = \int \frac{d\theta}{2\pi}\left(\gamma_1^o + \gamma_2^o \cos 2\theta\right) L_\gamma, \; L_\gamma = \log \frac{1}{|\gamma_1^o + \gamma_2^o \cos 2\theta|}.$$

Solving this set we obtain $\tilde{\Delta}_h$ and $r \equiv |\Delta_{e_2}/\Delta_{e_1}| = |\gamma_1/\gamma_2| \approx |\gamma_1^0/\gamma_2^0|$ as functions of α and β. Comparing the two functions, we identify $\tilde{\Delta}_h$ for which $r > 1$, i.e., when the gap along the electron FS has nodes.

Results. In Fig. 1(a) we show $\tilde{\Delta}_h$ for different α and β compared to the BCS value. The black line separates the regions of nodal and non-nodal gap ($r > 1$ and $r < 1$, respectively). The nodal region corresponds to larger values of α (i.e., larger angular dependence of the interaction) and larger β (i.e., larger intraband repulsion). There is a critical value $\beta_{\text{critical}} = 1/\sqrt{2}$ beyond which the gap remains nodal even when α is infinitesimally small.[30] In Fig. 1(b) we take the slices of Fig. 1(a) and show the trajectories of $\tilde{\Delta}_h$ for fixed values of r (for every given β, different r correspond to different values of α). We clearly see that there is a correlation between the magnitude of $\tilde{\Delta}_h$ and whether the gap along the

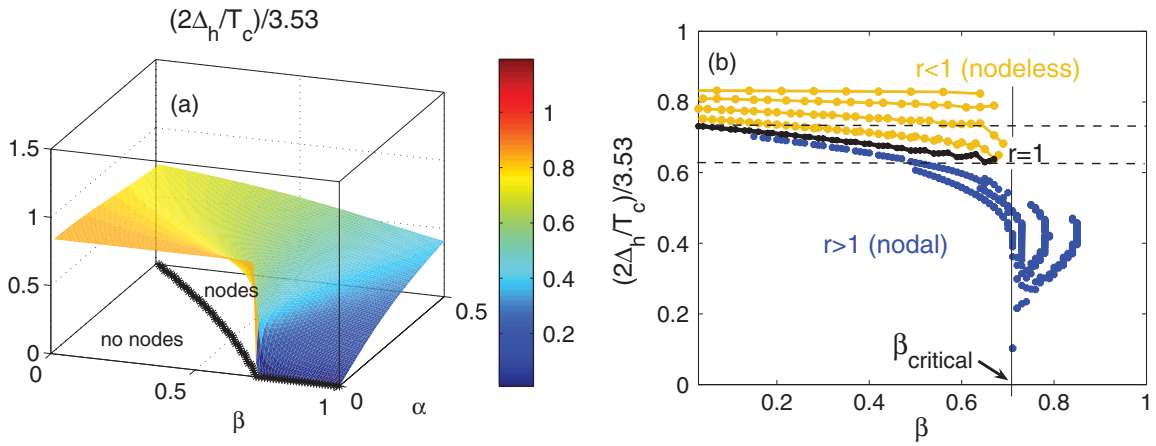

FIG. 1. (Color online) $2\Delta_h/T_c$ (relative to the BCS value) for the 4-pocket model A. (a) $2\Delta_h/T_c$ as a function of α and β. The black line separates nodal and nodeless regions. The colors indicate the gap magnitudes relative to the BCS value of 3.53. (b) $2\Delta_h/T_c$ vs β for different values of r. $r > 1$ [blue (dark gray)] are nodal lines, $r < 1$ [yellow (light gray)] are nodeless lines, and $r = 1$ (black) is the boundary line. The dashed lines indicate the boundaries of the "gray area" (see text). Outside of gray area the gap either definitely has nodes or is definitely non-nodal.

TABLE I. Table summarizing the main results for the 4- and 5-pocket models A and B (two equivalent hole FSs at (0,0) or one hole FS at (0,0), respectively). Δ_h corresponds to the largest hole gap in each model. The "gray-area" values are relative to the BCS value of 3.53. $2\Delta_h/T_c$, relative to the BCS value, and Δ_{e_1}/Δ_h values are listed for $\alpha \to 0, \beta \to 0$.

	Δ_{e_1}/Δ_h	$(2\Delta_h/T_c)/3.53$	Gray area	β_{critical}
4 pocket A	$-\sqrt{2}$	$2^{-1/4}$	0.63–0.73	$1/\sqrt{2}$
4 pocket B	$-1/\sqrt{2}$	$2^{1/4}$	0.94–1.04	$\sqrt{2}$
5 pocket A	-1	$2^{1/4}$	0.84–1.04	0.5
5 pocket B	-1	1	0.78–0.87	1

electron FS is nodal or has no nodes. Namely, for $\tilde{\Delta}_h$ above 0.73 the gap has no nodes, and for $\tilde{\Delta}_h$ below 0.63 the gap has nodes, no matter what α is. There is a "gray area" between 0.63 and 0.73 marked by dashed lines in the figure. For $\tilde{\Delta}_h$ in this area, the gap is either nodal or non-nodal, depending on α.

We found similar behavior for all cases that we studied. Namely, for $\tilde{\Delta}_h$ above some threshold, the corresponding gap along the electron FSs has no nodes, for $\tilde{\Delta}_h$ below some other threshold, electronic gaps have nodes, and there is some relatively narrow "gray area" in between the thresholds. In Table I we summarize the main results for the four models that we considered.

Comparison with experiments. A summary of the results is pictorially presented in "structure strips" in Fig. 2, where for each case we show $\tilde{\Delta}_h$ and its partition into the nodal, the nodeless, and the gray areas. We keep the upper boundary open because strong coupling effects are known to increase the value of $\tilde{\Delta}_h$.[31] The symbols represent the ARPES data for the gaps along the hole FSs. Since our objective is to set an upper bound on $\tilde{\Delta}_h$ for nodal behavior, we compare the largest of the hole gaps from the theory to the largest hole gap observed in the experiments.

For the electron-doped 122 material $Ba(Fe_{1-x}Co_x)_2As_2$, both theory and experiment indicate that there are two hole and two electron pockets. ARPES results suggest[24] that one hole pocket is near-nested with the electron pockets while the other is not. From our perspective, this should be close to our case of one hole and two electron pockets. We see that the measured $\tilde{\Delta}_h$ near the optimal doping sits well in the nodeless regime. This is consistent with the specific-heat and thermal-conductivity data, which indicate that the gap in optimally doped $Ba(Fe_{1-x}Co_x)_2As_2$ has no nodes.[13,32]

A similar situation holds for the electron-doped 1111 material $NdFeAsO_{0.9}F_{0.1}$. The measured Δ_h is around 15 meV[20] for high $T_c \approx 53$ K, which yields $2\Delta_h/T_c \approx 6.57$, well into the nodeless region. The non-nodal gap in high-T_c 1111 materials is consistent with penetration depth measurements[33] assuming that interpocket impurity scattering is relevant.[34] For 111 LiFeAs, which has two hole and two electron FSs, ARPES results[25,26] suggest that the measured $\tilde{\Delta}_h$ is either in the nodeless region or near the upper boundary of gray area, suggesting that the full gap has no nodes, if, indeed, LiFeAs is an $s^{\pm}$ superconductor (see Ref. 35). The non-nodal electron gap is consistent with penetration-depth and specific-heat experiments[15,26] that clearly show exponential behavior at low T.

For the hole-doped 122 material $Ba_{1-x}K_xFe_2As_2$, ARPES data show three hole FSs, consistent with the fact that these are hole-doped materials. The ARPES data for $\tilde{\Delta}_h$ vary. The data by Nakayama *et al.*[19] show that the highest $\tilde{\Delta}_h$ is rather large (about twice the BCS value), which places this material deep into the nodeless region, where the gap along electron FSs is almost angle-independent. There is no evidence of nodes in this material from other measurements.[36]

Finally, for isovalent doping in 122 $BaFe_2(As_{1-x}P_x)_2$, recent laser ARPES measurements[22] detected three near-equivalent and near-isotropic hole gaps with $\tilde{\Delta}_h \sim 0.85$. This places the material near the lower boundary of the gray area [see Fig. 2, 5 pocket model A], i.e., from our analysis, the measured $\tilde{\Delta}_h$ *implies that there must be nodes along the electron FSs.* This is in line with thermal conductivity and penetration depth measurements, which show behavior consistent with the nodes in $BaFe_2(As_{1-x}P_x)_2$.[18] We caution, however, that the same laser ARPES study[22] reported $\tilde{\Delta}_h \approx 0.52$ in $Ba_{1-x}K_xFe_2As_2$, much smaller than other

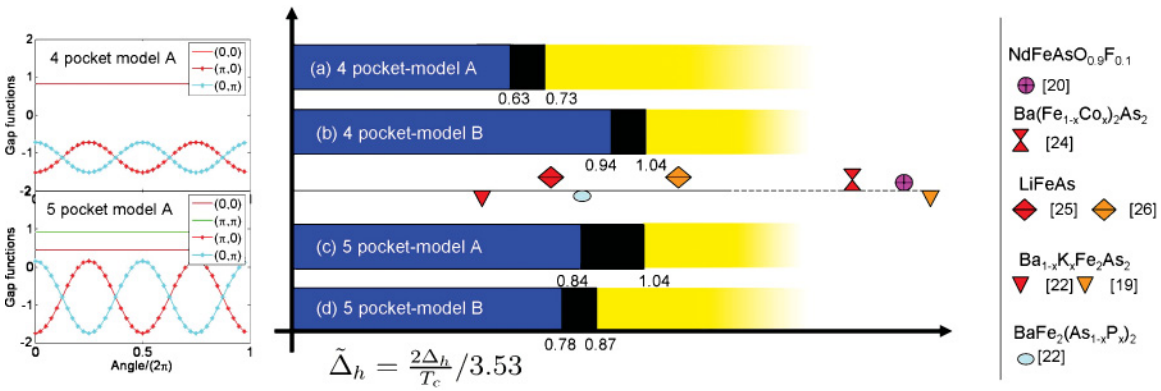

FIG. 2. (Color online) Gap structure strips for the 4- and 5-pocket models A and B. Each strip shows the regions of $2\Delta_h/T_c$ for the largest hole gap for which the gap along the electron FS definitely has nodes [blue (dark gray)], definitely has no-nodes [yellow (light gray)], or has/does not have nodes depending on α (gray). In the left panel, we show typical nodal and nodeless gap structures for A models. The symbols are the ARPES values for $2\Delta_h/T_c$. The symbols above the horizontal line should be compared with the 4-pocket models and those below the line with the 5-pocket models.

ARPES measurements. That value would imply nodes in $Ba_{1-x}K_xFe_2As_2$, in variance with what is known for this system.

Conclusions. The purpose of this work was to investigate whether one can predict, based on the measured $2\Delta_h/T_c$ along the hole FSs, whether the gaps on the electron FSs in FeSCs have nodes or not. The hole gaps have been measured by ARPES, but for most systems, ARPES measurements of the electron gaps separately on each of the two electron FSs are lacking. This issue is particularly relevant for systems like $BaFe_2(As_{1-x}P_x)_2$, in which penetration-depth and thermal-conductivity data show behavior consistent with the gap nodes.

We considered 4- and 5-pocket models with an angle-dependent interaction between hole and electron pockets and found that there is a direct correlation between $2\Delta_h/T_c$ on hole FSs and the strength of $\cos 2\theta$-oscillating-gap component on the electron FSs. If $2\Delta_h/T_c$ is larger than a certain value, there are no nodes, if it is smaller, then there must be nodes. There is a rather narrow range of $2\Delta_h/T_c$ near the boundary where the electron gap is either nodal or not depending on the strength of the $\cos 2\theta$ component of the interaction.

Most of ARPES data for Δ_h for near-optimally doped $NdFeAsO_{0.9}F_{0.1}$, $Ba(Fe_{1-x}Co_x)_2As_2$, $Ba_{1-x}K_xFe_2As_2$, and LiFeAs yield $2\Delta_h/T_c$ above the threshold, meaning that there should be no nodes along the electron FSs. This is consistent with the penetration-depth, thermal-conductivity, and specific-heat measurements in these materials. For p-doped $BaFe_2(As_{1-x}P_x)_2$, $2\Delta_h/T_c$ obtained by laser ARPES measurements is in the lower part of the gray area, meaning that the nodes on electron FSs are very likely. Detailed ARPES measurements of the electron gaps separately on the two hole FSs are clearly called for.

We acknowledge helpful discussions with R. Fernandes, P. Hirschfeld, I. Eremin, Y. Matsuda, and M. Vavilov. This work was supported by NSF-DMR-0906953.

[1] K. Kuroki *et al.*, Phys. Rev. Lett. **101**, 087004 (2008).
[2] Q. Si and E. Abrahams, Phys. Rev. Lett. **101**, 076401 (2008).
[3] P. A. Lee and X.-G. Wen, Phys. Rev. B **78**, 144517 (2008).
[4] I. I. Mazin *et al.*, Phys. Rev. Lett. **101**, 057003 (2008).
[5] T. Saito *et al.*, Phys. Rev. B **82**, 144510 (2010).
[6] S. Graser *et al.*, New J. Phys. **11**, 025016 (2009).
[7] C. Platt *et al.*, New J. Phys. **11**, 055058 (2009).
[8] F. Wang *et al.*, Phys. Rev. B **81**, 184512 (2010).
[9] V. Cvetkovic and Z. Tesanovic, Phys. Rev. B **80**, 024512 (2009).
[10] A. V. Chubukov, Physica C **469**, 640 (2009); A. V. Chubukov, D. Efremov, and I. Eremin, Phys. Rev. B **78**, 134512 (2008).
[11] R. M. Fernandes *et al.*, Phys. Rev. B **81**, 140501(R) (2010).
[12] A. D. Christianson *et al.*, Nature (London) **456**, 930 (2008).
[13] J.-Ph. Reid *et al.*, Phys. Rev. B **82**, 064501 (2010); M. A. Tanatar *et al.* Phys. Rev. Lett. **104**, 067002 (2010).
[14] R. T. Gordon *et al.*, Phys. Rev. B **82**, 054507 (2010); L. Luan *et al.*, Phys. Rev. Lett. **106**, 067001 (2011).
[15] H. Kim *et al.*, Phys. Rev. B **83**, 100502(R) (2011).
[16] G. Mu *et al.*, e-print arXiv:1103.1300.
[17] J. D. Fletcher *et al.*, Phys. Rev. Lett. **102**, 147001 (2009).
[18] K. Hashimoto *et al.*, Phys. Rev. B **81**, 220501(R) (2010).
[19] K. Nakayama *et al.*, Phys. Rev. B **83**, 020501 (2011); Y.-M. Xu, Nat. Phys. **7**, 198 (2011).
[20] T. Kondo *et al.*, Phys. Rev. Lett. **101**, 147003 (2008).
[21] D. V. Evtushinsky *et al.*, New J. Phys. **11**, 055069 (2009).
[22] T. Shimojima *et al.* (unpublished).
[23] Y. Sekiba *et al.*, New J. Phys. **11**, 025020 (2009).
[24] K. Terashima *et al.*, Proc. Natl. Acad. Sci. USA **106**, 7330 (2009)
[25] D. S. Inosov *et al.*, Phys. Rev. Lett. **104**, 187001 (2010).
[26] S. V. Borisenko *et al.*, Phys. Rev. Lett. **105**, 067002 (2010).
[27] D. S. Inosov *et al.*, e-print arXiv:1012.4041.
[28] S. Maiti *et al.*, e-print arXiv:1104.1814.
[29] S. Maiti and A. V. Chubukov, Phys. Rev. B **82**, 214515 (2010).
[30] A. V. Chubukov *et al.*, Phys. Rev. B **80**, 140515(R) (2009).
[31] D. J. Scalapino, Phys. Rep. **250**, 329 (1995); F. Marsiglio and J. P. Carbotte, in *The Physics of Conventional and Unconventional Superconductors*, edited by K. H. Bennemann and J. B. Ketterson (Springer-Verlag, Berlin, 2006).
[32] F. Hardy *et al.*, Europhys. Lett. **91**, 47008 (2010).
[33] C. Martin *et al.*, Phys. Rev. Lett. **102**, 247002 (2009).
[34] A. B. Vorontsov *et al.*, Phys. Rev. B **79**, 140507(R) (2009).
[35] B. Buechner *et al.* (unpublished).
[36] R. Khasanov *et al.*, Phys. Rev. Lett. **102**, 187005 (2009).